J. Fluid Mech. (1970), *vol.* 42, *part* 2, *pp.* 379–399
Printed in Great Britain

On edge effects in rheometry

By D. F. GRIFFITHS† AND K. WALTERS
Department of Applied Mathematics, University College of Wales, Aberystwyth

(Received 29 August 1969)

Consideration is given to the influence of edge effects on rheological measurements. To facilitate this, we discuss theoretically the flow generated by the slow steady rotation of a solid of revolution in an elastico-viscous liquid confined by convenient bath surfaces. The relevant linear partial differential equations are solved numerically. The simple problem of a rotating sphere and a concentric spherical container, for which an exact analytic solution is available, is first discussed to justify the method employed, and to indicate the necessary conditions to obtain a given accuracy. The numerical method is then applied to the case of a cone of finite dimensions rotating in a bath of elastico-viscous liquid. The predicted flow is shown to be in good agreement with experimental observations.

Application of the theory to rheogoniometric situations indicates that edge effects are not likely to be as significant as has been conjectured in the past.

1. Introduction

In an earlier paper (Griffiths, Jones & Walters 1969, referred to in the following as part 1), we indicated that edge effects in the flow of elastico-viscous liquids can have a strong influence on flow characteristics, and can, under some conditions, affect the whole of a flow field. Particular attention was paid to the parallel-plate geometry, and it was suggested tentatively that edge effects may have unwanted consequences in rheometry. In the present paper, we give detailed consideration to this suggestion, and investigate the importance of edge effects in rheological measurement. Particular attention will be paid to the cone-and-plate geometry, although reference will also be made to the parallel-plate case in the section dealing with viscosity and pressure measurements.

As in part 1, recourse is made to a numerical procedure to solve the flow problem. The basic equations of part 1 are first recast in terms of a spherical polar co-ordinate system, which is the appropriate system for the cone-and-plate geometry. We then discuss the numerical procedure for the case of a sphere rotating in an elastico-viscous liquid which fills a stationary concentric spherical container. Here, we have available an exact analytic solution for comparison (cf. Walters & Waters 1963; Waters 1964). This comparison justifies the numerical procedure and also indicates the number of step lengths (and hence

† Present address: Department of Mathematics, The University, Dundee, Scotland.

the 'computer time') required to obtain a given accuracy in the cone-and-plate problem.

The numerical method is then applied to the cone-and-plate geometry and the importance of edge effects in rheological measurement investigated. Where possible, the theoretical predictions are compared with experimental observations.

2. Basic equations

In the solution of rheological flow problems, the equations of motion and continuity have to be solved in conjunction with suitable equations of state. For the 'slow-flow' problems to be considered in the present paper, it is convenient to consider the so-called second-order equations, which may be written in the form (cf. part 1),

$$p_{ik} = -pg_{ik} + p'_{ik}, \tag{1}$$

$$p'_{ik} = 2\alpha_1 e^{(1)}_{ik} + 2\alpha_2 e^{(2)}_{ik} + 4\alpha_3 e^{(1)j} e^{(1)}_{jk}, \tag{2}$$

where p_{ik} is the stress tensor, g_{ik} the metric tensor of a suitable co-ordinate system, $e^{(1)}_{ik}$ the rate-of-strain tensor, $e^{(n)}_{ik} \equiv \vartheta^{n-1} e^{(1)}_{ik}/\vartheta t^{n-1}$ is called the nth rate-of-strain tensor, $\vartheta/\vartheta t$ being the convected time derivative introduced by Oldroyd (1950). α_1, α_2 and α_3 are material constants and (confining attention to incompressible fluids) p is an arbitrary isotropic pressure. In (1) and (2), covariant suffices are written below, contravariant suffices above, and the usual summation convention for repeated suffices is implied.

Partial justification for using the 'order' equations in the type of problem under consideration was given in part 1. We shall see that, in some rheometrical situations, they may be considered to be sufficiently general to allow quantitative predictions to be made (cf. § 4 (iii)), while in others the predictions are of a more tentative and qualitative nature (cf. § 4 (iv)).

We shall refer all physical quantities to spherical polar co-ordinates (r, θ, ϕ), $\theta = 0$ representing the (vertical) axis of rotation of the sphere in § 3 and the cone in § 4. U, V and W will denote the physical components of the velocity vector in the r, θ, ϕ directions, respectively.

It is convenient to introduce dimensionless variables (cf. Thomas & Walters 1964; Walters & Waters 1968, p. 211)†

$$\left.\begin{aligned} U &= \frac{\nu u}{a}, \quad V = \frac{\nu v}{a}, \quad W = \Omega a w, \\ p &= \rho g r \cos\theta + \frac{\rho \nu^2}{a^2} p^*, \quad r = a r_1, \\ p'_{(ik)} &= \frac{\alpha_1 \nu}{a^2} \begin{bmatrix} p''_{(r_1 r_1)} & p''_{(r_1 \theta)} & (\Omega a^2/\nu)\, p''_{(r_1 \phi)} \\ p''_{(\theta r_1)} & p''_{(\theta\theta)} & (\Omega a^2/\nu)\, p''_{(\theta\phi)} \\ (\Omega a^2/\nu)\, p''_{(\phi r_1)} & (\Omega a^2/\nu)\, p''_{(\phi\theta)} & p''_{(\phi\phi)} \end{bmatrix}, \end{aligned}\right\} \tag{3}$$

where $\nu = \alpha_1/\rho$, a is a typical length, g the acceleration due to gravity, ρ the density of the fluid, and Ω is the angular velocity of the sphere in § 3 and the

† Brackets placed round suffices are used to denote *physical* components of tensors.

cone in § 4. Substituting (3) into the stress equations of motion and the equation of continuity, we obtain for steady axially-symmetric flow:

$$u\frac{\partial u}{\partial r_1}+\frac{v}{r_1}\frac{\partial u}{\partial \theta}-\frac{v^2}{r_1}-\frac{Lw^2}{r_1}=-\frac{\partial p^*}{\partial r_1}+\frac{1}{r_1^2}\frac{\partial}{\partial r_1}(r_1^2 p''_{(r_1 r_1)}) + \frac{1}{r_1\sin\theta}\frac{\partial}{\partial\theta}(\sin\theta\, p''_{(r_1\theta)})-\frac{p''_{(\theta\theta)}}{r_1}-\frac{p''_{(\phi\phi)}}{r_1}, \quad (4)$$

$$\frac{u}{r_1}\frac{\partial}{\partial r_1}(r_1 v)+\frac{v}{r_1}\frac{\partial v}{\partial\theta}-\frac{Lw^2}{r_1}\cot\theta=-\frac{1}{r_1}\frac{\partial p^*}{\partial\theta}+\frac{1}{r_1^3}\frac{\partial}{\partial r_1}(r_1^3 p''_{(r_1\theta)}) + \frac{\partial(\sin\theta\, p''_{(\theta\theta)})}{r_1\sin\theta\,\partial\theta}-\frac{p''_{(\phi\phi)}}{r_1}\cot\theta, \quad (5)$$

$$\frac{u}{r_1}\frac{\partial}{\partial r_1}(r_1 w)+\frac{v}{r_1\sin\theta}\frac{\partial}{\partial\theta}(w\sin\theta)=\frac{1}{r_1^3}\frac{\partial}{\partial r_1}(r_1^3 p''_{(r_1\phi)})+\frac{1}{r_1\sin^2\theta}\frac{\partial}{\partial\theta}(\sin^2\theta\, p''_{(\theta\phi)}), \quad (6)$$

$$\frac{\partial}{\partial r_1}(u r_1^2\sin\theta)+\frac{\partial}{\partial\theta}(v r_1\sin\theta)=0, \quad (7)$$

where

$$L=\left(\frac{\Omega a^2}{\nu}\right)^2, \quad (8)$$

i.e. the square of a Reynolds number.

Since we are interested in slow-flow situations, we obtain a solution of (1), (2), and (4)–(7) by expanding the velocity components and the pressure in ascending powers of L, as follows:

$$\left.\begin{aligned} U &= \frac{\nu}{a}[Lu_1+L^2u_2+\ldots],\\ V &= \frac{\nu}{a}[Lv_1+L^2v_2+\ldots],\\ W &= \Omega a r_1\sin\theta[w_0+Lw_1+\ldots],\\ p-\rho g r\cos\theta &= \frac{\rho\nu^2}{a^2}[Lp_1^*+L^2p_2^*+\ldots]. \end{aligned}\right\} \quad (9)$$

From (7), it is convenient to define a stream function χ, such that

$$u=-\frac{1}{r_1^2\sin\theta}\frac{\partial\chi}{\partial\theta}, \quad v=\frac{1}{r_1\sin\theta}\frac{\partial\chi}{\partial r_1}, \quad (10)$$

and we write

$$\chi=L\chi_1+L^2\chi_2+\ldots.$$

From (2), (6) and (9), it can easily be shown that the equation for w_0 (which corresponds to the solution when terms of order L are neglected) is

$$\left(\nabla_1^2-\frac{1}{r_1^2\sin^2\theta}\right)w_0 r_1\sin\theta=0, \quad (11)$$

where

$$\nabla_1^2\equiv\frac{1}{r_1^2}\frac{\partial}{\partial r_1}\left(r_1^2\frac{\partial}{\partial r_1}\right)+\frac{1}{r_1^2\sin\theta}\frac{\partial}{\partial\theta}\left(\sin\theta\frac{\partial}{\partial\theta}\right). \quad (12)$$

The equation for the first-order stream function χ_1 can be obtained from (4), (5) and (9)–(12) in the form,

$$D^4\chi_1 = 2r_1\sin^2\theta w_0\left[\frac{\partial w_0}{\partial\theta}\sin\theta - \frac{\partial w_0}{\partial r_1}r_1\cos\theta\right] + E(w_0), \tag{13}$$

where

$$D^2 \equiv \frac{\partial^2}{\partial r_1^2} + \frac{\sin\theta}{r_1^2}\frac{\partial}{\partial\theta}\left(\frac{1}{\sin\theta}\frac{\partial}{\partial\theta}\right), \tag{14}$$

$$\begin{aligned} E(w_0) = \sin\theta\Bigg[\frac{\partial}{\partial\theta}\Bigg\{(2\alpha_2'+\alpha_3')\Bigg[\frac{\partial}{\partial r_1}\left(r_1^4\sin^2\theta\left(\frac{\partial w_0}{\partial r_1}\right)^2\right) + \frac{1}{r_1\sin\theta}\frac{\partial}{\partial\theta}\left(r_1\sin^3\theta\frac{\partial w_0}{\partial r_1}\frac{\partial w_0}{\partial\theta}\right) \\ - \frac{\sin^2\theta}{r_1}\left(\frac{\partial w_0}{\partial\theta}\right)^2\Bigg] - \frac{\alpha_3'}{r_1}\left[r_1^2\left(\frac{\partial w_0}{\partial r_1}\right)^2 + \left(\frac{\partial w_0}{\partial\theta}\right)^2\right]\sin^2\theta\Bigg\} - \frac{\partial}{\partial r_1}\Bigg\{(2\alpha_2'+\alpha_3') \\ \times\left[r_1\frac{\partial}{\partial r_1}\left(r_1^4\sin^2\theta\frac{\partial w_0}{\partial r_1}\frac{\partial w_0}{\partial\theta}\right) + \frac{1}{\sin\theta}\frac{\partial}{\partial\theta}\left(\sin^3\theta\left(\frac{\partial w_0}{\partial\theta}\right)^2\right)\right] - \alpha_3'\sin\theta\cos\theta \\ \times\left[r_1^2\left(\frac{\partial w_0}{\partial r_1}\right)^2 + \left(\frac{\partial w_0}{\partial\theta}\right)^2\right]\Bigg\}\Bigg], \end{aligned} \tag{15}$$

and $\alpha_2' = \alpha_2/\rho a^2$, $\alpha_3' = \alpha_3/\rho a^2$. E is the contribution to the equation due to the elasticity in the fluid.

Equations (11) and (13) correspond to (14) and (19) of part 1, which were derived in somewhat more detail for a *cylindrical* polar co-ordinate system.

3. Flow due to a rotating sphere

We first consider the problem of a sphere of radius a rotating with angular velocity Ω about a vertical diameter in an elastico-viscous liquid which is contained in a stationary concentric spherical container of radius βa ($\beta > 1$). The appropriate boundary conditions are

$$\left.\begin{aligned} &w_0 = 1 \quad \text{on} \quad r_1 = 1, \quad w_0 = 0 \quad \text{on} \quad r_1 = \beta, \\ &\chi_1 = \text{const.}, \quad \frac{\partial\chi_1}{\partial r_1} = 0 \quad \text{on} \quad r_1 = 1 \quad \text{and} \quad r_1 = \beta. \end{aligned}\right\} \tag{16}$$

Analytic solutions of (11) and (13), subject to (16), have been given by Walters & Waters (1963), and we shall find it convenient to refer to these for comparison purposes. (Also see Waters 1964.)

To solve (11) and (13) numerically, we first write the fourth-order equation in 'split-operator' form. The problem then reduces to one of solving a series of coupled second-order elliptic partial differential equations. These equations can be discretized to produce symmetric matrix equations, which are solved by successive line over-relaxation. Further details of the numerical procedure may be found in part 1.

The relevant grid for the rotating-sphere problem is defined by the lines,

$$\left.\begin{aligned} r_1 &= 1 + i\Delta r, \qquad i = 0, 1, 2 \ldots n+1, \\ \theta &= j\Delta\theta, \qquad\quad j = 0, 1, 2 \ldots m+1, \end{aligned}\right\} \tag{17}$$

$$\left.\begin{aligned} &\text{where} && \Delta r = (\beta-1)/(n+1), \\ &\text{and} && \Delta\theta = \pi/(m+1). \end{aligned}\right\} \tag{18}$$

The intersection of the lines given by (17) are called nodal points and are denoted by P_N. If R represents the domain,

$$\left.\begin{aligned} &1 < r_1 < \beta, \\ &0 < \theta < \pi, \end{aligned}\right\} \tag{19}$$

and ∂R its boundary, then R_Δ and ∂R_Δ are the sets of nodal points belonging to R and ∂R, respectively. From (17), (18) and (19), it is clear that the only intersections of ∂R with grid lines are at nodal points.

The computed numerical solution for the primary flow velocity $\overline{w}\,(= w_0 r_1 \sin\theta)$ is given in figure 1. Also included is the exact analytic solution given by Walters & Waters (1963). It is seen that the two are indistinguishable.

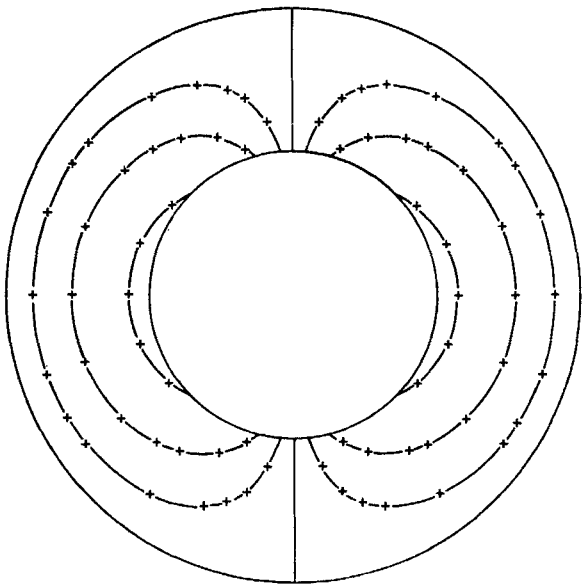

FIGURE 1. Curves of constant primary flow velocity $\overline{w}$ for $\beta = 2$: +, numerical solution ($\Delta r = \frac{1}{10}$, $\Delta\theta = \pi/20$); −, analytic solution.

If $\tilde{w}(P_N)$ represents the analytic solution for $\overline{w}$ at the node P_N and $w(P_N)$ the corresponding numerical solution, a suitable measure of the relative difference between $\tilde{w}$ and w is the function ξ defined by

$$\xi = \frac{\left[\sum_{P_N \in R_\Delta} [\tilde{w}(P_N) - w(P_N)]^2\right]^{\frac{1}{2}}}{\left[\sum_{P_N \in R_\Delta} [\tilde{w}(P_N)]^2\right]^{\frac{1}{2}}}. \tag{20}$$

Even for relatively coarse meshes ($\Delta r = \frac{1}{10}$, $\Delta\theta = \pi/20$), ξ is of the order of 6×10^{-4}, which indicates that accurate finite-difference solutions to the second-order equation (11) are easily obtainable.

The numerical method of part 1 has also been used to solve (13). The relevant results are summarized in figures 2–5, which contain analytic and numerical secondary-flow (i.e. $\chi_1 =$ constant) curves for various values of α_2' and α_3'.† Figures 2(*a*)–5(*a*) are based on the analytic solution and may be compared with similar curves given by Waters (1964). We see that at least four types of flow behaviour are possible, depending on the precise values of α_2' and α_3'.‡ Figures 2(*b*)–5(*b*) contain curves based on the numerical solution for a relatively coarse

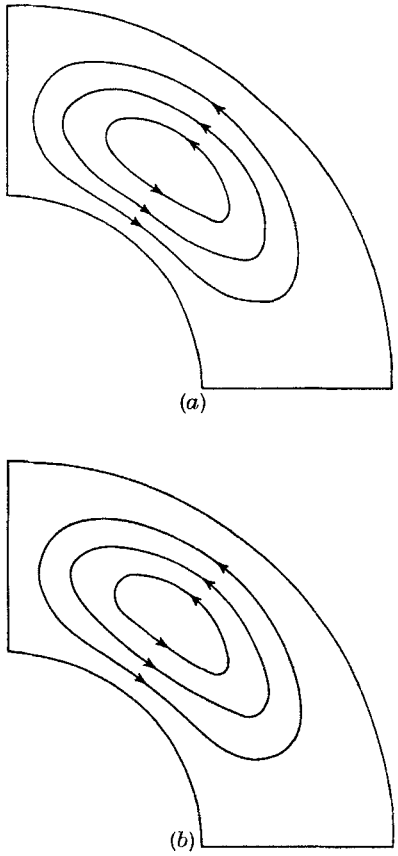

FIGURE 2

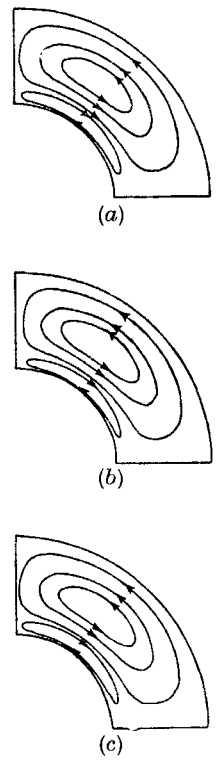

FIGURE 3

FIGURE 2. Streamline projections for $\beta = 2$ and $\alpha_2' + \alpha_3' = 0$. (*a*) Analytic curves for convenient values of χ_1. (*b*) Numerical curves ($\Delta r = \frac{1}{10}$, $\Delta\theta = \pi/20$) for the same values of χ_1.

FIGURE 3. Streamline projections for $\beta = 2$ and $\alpha_2' + \alpha_3' = 0{\cdot}055$. (*a*) Analytic curves for convenient values of χ_1. (*b*) Numerical curves ($\Delta r = \frac{1}{20}$, $\Delta\theta = \pi/20$) for the same values of χ_1. (*c*) Numerical curves ($\Delta r = \frac{1}{60}$, $\Delta\theta = \pi/20$) for the same values of χ_1 used in (*a*) and (*b*).

† It may be deduced on theoretical grounds that α_2' is negative, and from experimental results that the most likely range of α_3' is $-2\alpha_2' \leqslant \alpha_3' < -2{\cdot}5\alpha_2'$. We have verified that varying α_3' between these limits does not significantly affect the general shape of the streamlines, and we take $\alpha_3' = -2\alpha_2'$ throughout.

‡ In the analytic solution, it is the combination $\alpha_2' + \alpha_3'$ which determines the type of flow behaviour (cf. Walters & Waters 1963).

mesh and figures 3(*c*) and 4(*c*) correspond to a finer grid when the flow field is divided into two and three regions, respectively.† We see that the coarser nets predict the general form of the flow patterns and that the agreement between the analytic and numerical solutions improves noticeably with increasing n in figure 4.

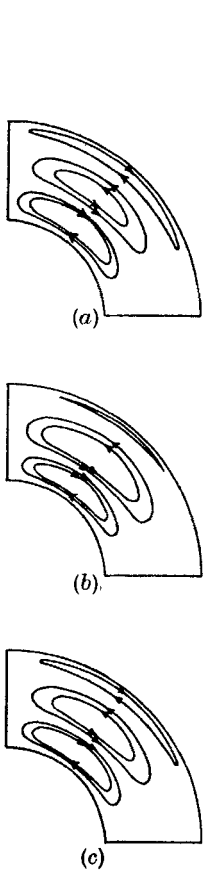

FIGURE 4

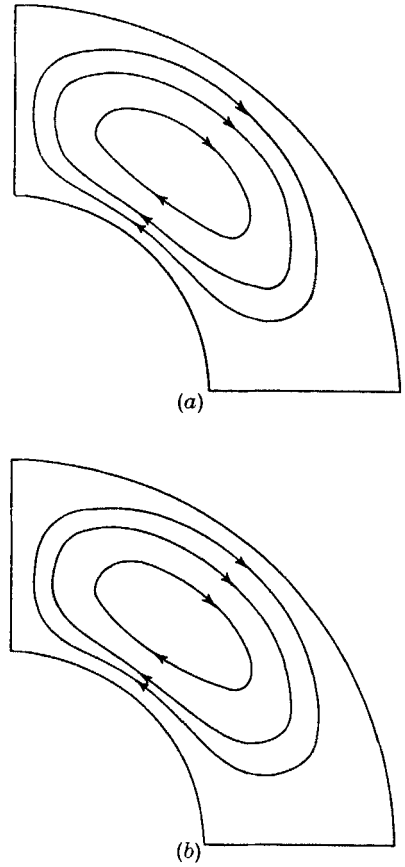

FIGURE 5

FIGURE 4. Streamline projections for $\beta = 2$ and $\alpha_2' + \alpha_3' = 0{\cdot}0564$. (*a*) Analytic curves for convenient values of χ_1. (*b*) Numerical curves ($\Delta r = \frac{1}{20}$, $\Delta\theta = \pi/20$) for the same values of χ_1. (*c*) Numerical curves ($\Delta r = \frac{1}{60}$, $\Delta\theta = \pi/20$) for the same values of χ_1 used in (*a*) and (*b*).

FIGURE 5. Streamline projections when $\beta = 2$ and $\alpha_2' + \alpha_3' = 0{\cdot}1$. (*a*) Analytic curves for convenient values of χ_1. (*b*) Numerical curves ($\Delta r = \frac{1}{20}$, $\Delta\theta = \pi/20$) for the same values of χ_1.

To elucidate the effect of the number of step lengths on the accuracy of the solution, we plot, in figure 6, ξ as a function of n for the values of α_2' and α_3' considered in figures 2–5. The number of step lengths required to give a particular accuracy is seen to increase significantly with the number of regions in the flow

† In most of the numerical work, we took a constant step length in the θ direction ($\Delta\theta = \pi/20$) and varied Δr, since we found that making Δr smaller reduces the error much more than altering $\Delta\theta$ by an equivalent amount.

field. For example, a 2 % accuracy in the case of one region (cf. figures 2 and 5) requires 10 steps, in the case of two regions (figure 3) requires 50 steps, and for three regions (figure 4) requires as many as 100 step lengths.

The work of § 3 indicates that the numerical method under consideration is able to predict the flow to any desired accuracy when a solid of revolution is rotated slowly in an elastico-viscous liquid. It also shows that the size of the mesh required to give a particular accuracy is very dependent on the form of the solution.

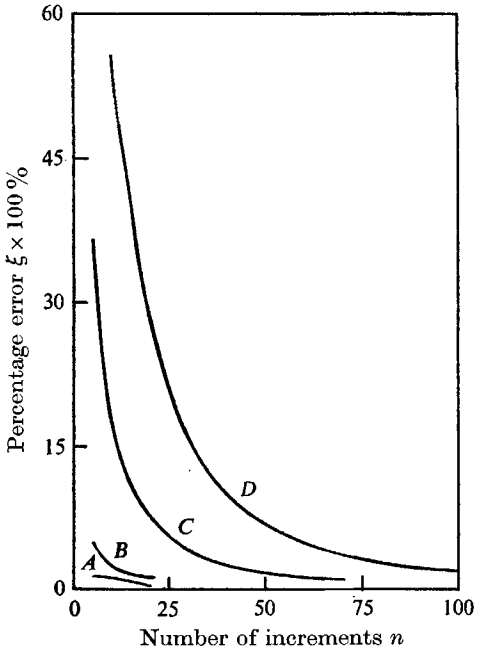

FIGURE 6. Variation of the error function ξ, defined in terms of the stream function χ_1, with n when $\Delta\theta = \pi/20$ and A, $\alpha_2'+\alpha_3' = 0$, B, $\alpha_2'+\alpha_3' = 0{\cdot}1$, C, $\alpha_2'+\alpha_3' = 0{\cdot}055$, D, $\alpha_2'+\alpha_3' = 0{\cdot}0564$.

4. Flow due to a rotating cone

(i) *Introduction*

Measurements of the response of an elastico-viscous liquid, when sheared in the gap between a rotating cone and a stationary plate, are often used in the characterization of the non-Newtonian properties of the material. The interpretation of such measurements is based on a theory which assumes that both the cone and the plate are of infinite extent (Giesekus 1967; Walters & Waters 1968). Section 4 is devoted to a study of the validity of this assumption. In order to do this, we consider the flow due to the slow steady rotation of a cone of finite radius when it is immersed in a bath containing an elastico-viscous liquid. Owing to the complicated shape of the boundary (see figure 7) analytic methods cannot be used, and we resort to the numerical procedure described in part 1 and employed in § 3. We attempt to remain within the limits of grid size imposed by the conclusions of § 3, so that we may have confidence in the results.

The basic equations (11) and (13) are solved over the domain R shown in figure 7. The boundary of ∂R of R may be conveniently divided into three parts, ∂R_1, ∂R_2 and ∂R_3, where ∂R_1 refers to OAB, ∂R_2 to BC and ∂R_3 to ODC. ∂R_1 then represents the surface of the cone, ∂R_3 a convenient bath surface and ∂R_2 is assumed to be at a sufficient distance from the edge A to ensure that the primary velocity is the same as that for the concentric-spheres problem (§ 3). We further assume that there is no secondary flow across this line, i.e. ∂R_2 is a streamline. This assumption is introduced so that, when the gap angle θ_0 is small, there is a sufficient proportion of grid points in the important region below the cone.

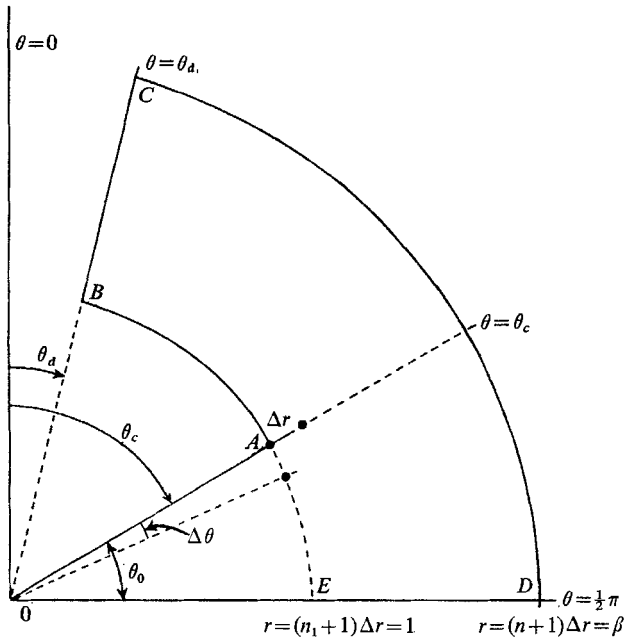

FIGURE 7. Domain of integration for the rotating-cone problem.

The boundary conditions on $\overline{w}$ are now

$$\left.\begin{aligned} \overline{w} &= r_1 \sin\theta \quad \text{on} \quad \partial R_1, \\ \overline{w} &= \left(\frac{C}{r_1^2} + Dr_1\right)\sin\theta \quad \text{on} \quad \partial R_2, \\ \overline{w} &= 0 \quad \text{on} \quad \partial R_3, \end{aligned}\right\} \tag{21}$$

where $D = 1/(1-\beta^3)$, $C = -\beta^3 D$ and β is the radius of the bath ($= OD$). The boundary condition on ∂R_2 is, of course, obtained from the *analytic* solution of the concentric-spheres problem for convenience.

The boundary conditions on χ_1 are

$$\chi_1 = \frac{\partial \chi_1}{\partial n} = 0 \quad \text{on} \quad \partial R, \tag{22}$$

where $\partial/\partial n$ denotes the normal derivative to the boundary.

In order to solve (11) and (13) subject to (21) and (22), we first define a grid of co-ordinate lines on R. This is done in an analogous fashion to that described in § 3. By placing a 'spherical cap' on top of the cone we have a domain whose boundaries are all parallel to co-ordinate surfaces.† To ensure that the boundary coincides with grid lines we define the integers n, n_1, m, m_1 such that

$$\left.\begin{aligned}(m_1+1)\,\Delta\theta+\theta_d &= \theta_c,\\ (m+1)\,\Delta\theta+\theta_d &= \pi/2,\\ (n_1+1)\,\Delta r &= 1,\\ (n+1)\,\Delta r &= \beta,\end{aligned}\right\} \tag{23}$$

where, in the non-dimensionalization (3), we have taken the typical length a to be the radius of the cone.

It will be of interest later to compute the couple on the rotating cone and the pressure distribution on the stationary plate. The couple C is given by

$$C = 2\pi \sin^2\theta_c \int_0^a r^2 p_{(\theta\phi)}|_{\theta=\theta_c}\, dr. \tag{24}$$

If we assume that the flow is sufficiently slow, we may neglect terms of order L, and we have, from (1), (2), (9) and (24),

$$C = 2\pi\Omega a^3 \alpha_1 I_N, \tag{25}$$

where I_N is the non-dimensional integral,

$$I_N = \sin^3\theta_c \int_0^1 r_1^2 \left.\frac{\partial w_0}{\partial\theta}\right|_{\theta=\theta_c} dr_1. \tag{26}$$

The pressure on the plate is given by (cf. equation (9))

$$p|_{\theta=\pi/2} = \Omega^2 a^2 \rho p_1^*, \tag{27}$$

where, from (2), (4), (9) and (21), p_1^* is given by the first-order differential equation.

$$\left.\frac{\partial p_1^*}{\partial r_1}\right|_{\theta=\pi/2} = -\frac{1}{r_1^2}\frac{\partial}{\partial\theta}(D^2\chi_1)\Big|_{\theta=\pi/2} + (2\alpha_2'+\alpha_3')\frac{\partial}{\partial\theta}\left(\frac{\partial w_0}{\partial r_1}\frac{\partial w_0}{\partial\theta}\right)\Big|_{\theta=\pi/2} - 2\left(\frac{\alpha_2'+\alpha_3'}{r_1}\right)\left(\frac{\partial w_0}{\partial\theta}\right)^2\Big|_{\theta=\pi/2}. \tag{28}$$

Further, the normal stress component $[-p_{(\theta\theta)}]_{\theta=\pi/2}$ on the stationary plate is, from (1), (2), (9) and (22),

$$[-p_{(\theta\theta)}]_{\theta=\pi/2} = p|_{\theta=\pi/2} - (2\alpha_2+\alpha_3)\,\Omega^2\left(\frac{\partial w_0}{\partial\theta}\right)^2\Big|_{\theta=\pi/2} - 2\Omega^2\rho a^2\Psi, \tag{29}$$

where the non-dimensional function Ψ is given by

$$\Psi = \frac{1}{r_1^2}\left.\frac{\partial^2\chi_1}{\partial r_1\,\partial\theta}\right|_{\theta=\pi/2}. \tag{30}$$

† The effect of the spherical cap on the flow between the cone and the plate will be considered later.

For completeness, we note that the expressions for the stream function χ_1 and the pressure on the plate $[-p_{(\theta\theta)}]_{\theta=\pi/2}$ would be the same if we had considered the *third*-order equations instead of the second-order equations (2). The expression for the couple C would, however, be modified (cf. Walters & Waters 1968).

(ii) *Analytic theory based on an infinite cone and plate system*

The analytic theory based on an infinite cone and plate has been considered by Bhatnagar & Rathna (1962), Mohan Rao (1962), Giesekus (1967), and Walters & Waters (1968). In this case, (11) and (13) have to be solved subject to

$$\left.\begin{aligned} \bar{w} &= r_1 \sin\theta, \quad \text{on} \quad \theta = \theta_c, \\ \bar{w} &= 0, \quad\quad\ \text{on} \quad \theta = \pi/2, \end{aligned}\right\} \tag{31}$$

$$\frac{\partial \chi_1}{\partial r_1} = \frac{\partial \chi_1}{\partial \theta} = 0, \quad \text{on} \quad \theta = \theta_c \quad \text{and} \quad \theta = \pi/2. \tag{32}$$

A solution to the problem exists in the form,

$$\bar{w} = w_0 r_1 \sin\theta, \tag{33}$$

$$\chi_1 = r_1^5 f(\theta) + (\alpha_2' + \alpha_3') r_1^3 g(\theta), \tag{34}$$

where w_0 is given by

$$w_0 = A_1 \left(\ln \tan \frac{\theta}{2} - \cot\theta \operatorname{cosec}\theta \right), \tag{35}$$

and

$$A_1 = 1 \Big/ \left(\ln \tan \frac{\theta_c}{2} - \cot\theta_c \operatorname{cosec}\theta_c \right). \tag{36}$$

$f(\theta)$ and $g(\theta)$ are the solutions of certain fourth-order ordinary differential equations which are independent of the material parameters. These have been tabulated for various gap angles by Walters & Waters (1968).

The relevant analytic expressions for the couple and the normal pressure are

$$C = 2\pi\Omega a^3 \alpha_1 I_A, \tag{37}$$

where

$$I_A = -\tfrac{2}{3} A_1, \tag{38}$$

and

$$[-p_{(\theta\theta)}]_{\theta=\pi/2} = -\frac{\Omega^2}{2}\rho(r^2 - a^2)\left(\frac{d^3 f}{d\theta^3}\right)_{\theta=\pi/2} - \Omega^2(\alpha_2 + \alpha_3) \times \left\{ \left(\frac{d^3 g}{d\theta^3}\right)_{\theta=\pi/2} + 8A_1^2 \right\} \ln\left(\frac{r}{a}\right) + p_a, \tag{39}$$

where p_a is the pressure at $r = a$.

(iii) *Flow situations for wide-gap angles*

Wide-gap situations are of interest for two reasons. First, they enable us to demonstrate the secondary-flow patterns which may be formed, and secondly they are useful in simulating experimental configurations which are sometimes used for rheometric measurements (see, e.g. Giesekus 1967). In these wide-gap situations, the theoretical analysis has predictive value, since the experimental conditions usually fall within the range of the theoretical approximations.

Figure 8 contains theoretical curves of constant primary flow velocity $\overline{w}$ determined numerically for $\theta_c = 60°$. These are independent of the material constants and hence need only be computed once for any given domain. For purposes of comparison, we have also included the corresponding curves obtained from the analytic solution given by (35) and (36). We see that the analytic and numerical curves show the expected departure near the edge of the cone.

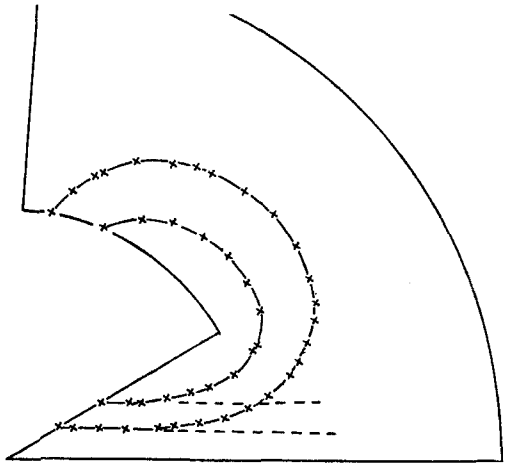

FIGURE 8. Curves of constant primary-flow velocity $\overline{w}$ for $\theta_0 = 30°$: —×—, numerical solution ($\Delta r = \frac{1}{10}$, $\Delta\theta = \pi/20$); – – –, analytic curves obtained from the 'infinite cone' theory.

The three major types of secondary flow, which may be obtained from the numerical solution of (13) by variation of α_2' and α_3', are illustrated in figure 9. Figure 9(*a*) contains the streamlines for a Newtonian fluid ($\alpha_2' = \alpha_3' = 0$) which are seen to be directed outwards at the rotating cone and inwards at the stationary plate. On changing the values of the constants to $\alpha_2' = -0{\cdot}04$ and $\alpha_3' = 0{\cdot}08$, the flow pattern changes considerably (figure 9(*b*)). The regions, which occur in the gap between the cone and the plate, can be considered to be the result of different influences. The dominating forces in these regions, taken in the order in which they occur radially from the vertex outwards, are: elastic, inertial, those due to edge effects, followed by patterns influenced by the shear flow between the spherical boundaries. It is seen, therefore, that edge effects can affect a large proportion of the flow field.

By further changing the material constants to $\alpha_2' = -0{\cdot}5$, $\alpha_3' = 0{\cdot}1$, the flow field becomes governed by elastic forces with no intermediate inertial region. The streamline patterns are very similar to those for a Newtonian liquid, except that their direction is changed. This is shown in figure 9(*c*).

In order to demonstrate that the predicted flow patterns of figure 9 can be obtained in practice, we carried out a number of simple experiments using an experimental arrangement similar to that discussed in part 1. This consisted of a bakelite cone of semi-vertical angle 60°, and slant height 5·6 cm, which could be rotated about its axis of symmetry. A spherical cap, of radius equal to the

slant height of the cone, could be placed on top of it if required. The cone was rotated by means of a rod attached in line with its axis of symmetry, the other end being connected to a motor-driven dynamometer.

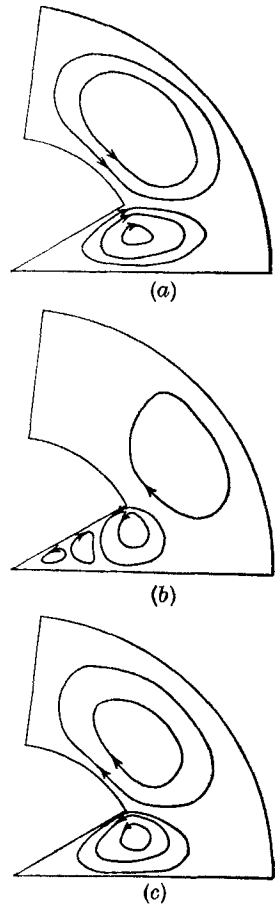

FIGURE 9. Streamline projections when $\theta_0 = 30°$ and (*a*) $\alpha_2' = \alpha_3' = 0$ ($\Delta r = \frac{1}{20}$, $\Delta\theta = \pi/20$), (*b*) $\alpha_2' = -0{\cdot}04$, $\alpha_3' = 0{\cdot}08$ ($\Delta r = \frac{1}{20}$, $\Delta\theta = \pi/20$), (*c*) $\alpha_2' = -0{\cdot}5$, $\alpha_3' = 1{\cdot}0$ ($\Delta r = \frac{1}{20}$, $\Delta\theta = \pi/20$).

The cone was submerged in the test solution, which was contained in a perspex tank. It was rotated with its vertex almost touching the bottom of the tank, and the streamlines formed in the expanse of liquid between the cone and plate were studied. The streamlines were rendered visible by means of blue dye. The three fluids used in the experiments were glycerol, which is purely viscous, and two elastico-viscous liquids, which were chosen to be 1·5 and 3·0 % aqueous solutions of polyacrylamide.† The viscosity of the glycerol was about 15 poises and the limiting viscosities (α_1) of the elastico-viscous liquids were approximately 8 poises and 50 poises for the 1·5 and 3·0 % solutions, respectively. The first

† Polyacrylamide P250 supplied by Cyanamide of Great Britain.

experiment was performed using the purely viscous liquid. The streamlines were observed at various rotational speeds and were seen to be directed outwards at the rotating cone, downwards to the bottom of the tank and inwards to the vertex (figure 10, plate 1).

Figures 11 (plate 2) and 13 (plate 3) contain the flow patterns for the two aqueous solutions for polyacrylamide, the rotational speed of the cone being 6 rev/min in both cases. The directions of the streamlines are the same as in figures 9(*b*) and 9(*c*), and it is clear that the theory yields a satisfactory description of the complex flow patterns.

Figure 12 (plate 2) contains the flow patterns observed when the cone, this time without the cap, was rotated in the same 1·5 % solution as that used in figure 11. Since the flow patterns shown in figures 11 and 12 are very similar, we conclude that this type of flow pattern is not due to the shape of the edge, but simply to its existence. This is taken as a justification for taking the particular domain shown in figure 7.

Measurements of the radius of the bounding surface between the elastic and inertial regions are often used in the characterization of elastico-viscous liquids and in particular in the determination of the second-order parameter combination $\alpha_2+\alpha_3$ (cf. equation (34), and see e.g. Giesekus 1967). The interpretation of the results is, however, based on an *infinite* cone-and-plate system (Giesekus 1967; Walters & Waters 1968), and this cannot take account of edge effects. We shall now investigate the influence of these effects on such measurements.

In view of the rapid spatial oscillations of the stream function in the flow patterns which occur in these situations, and also the conclusions reached in § 3, it is seen that, in order to achieve a sufficiently accurate numerical solution, great care must be taken to ensure that the number of grid points is chosen in accordance with the results contained in figure 6. For this reason, a complete account of edge effects on the bounding radius has not been possible. However, it is possible to give some idea of edge effects in this type of measurement by considering some illustrative examples.

Figure 14 contains streamline projections computed numerically for $\alpha_2' = -0{\cdot}03125$ and $\alpha_3' = 0{\cdot}0625$. Also given is the bounding region calculated for the infinite-cone case from the results of Walters & Waters (1968). It is seen that there is a measurable edge effect.

More quantitative results are contained in the following table which gives the percentage difference in bounding region based on the finite and infinite-cone situations. The values of $\alpha_2'+\alpha_3'$ used are those which divide the flow field

α_2'	α_3'	Percentage difference in bounding radius
−0·02875	0·0575	5·48
−0·03	0·06	6·20
−0·03125	0·0625	7·03

TABLE 1

in the finite cone case into three regions of roughly the same size (measured radially).

We would expect the percentage difference to be smaller for smaller values of α_2', since the elastic region would be smaller and therefore further from the edge. We can also anticipate a rapid increase in percentage difference as α_2' is increased, and, when the intermediate region disappears (as in figures 9(*c*) and 13), no interpretation of experimental results on the basis of an infinite cone is possible.

We may conclude, therefore, that, so long as the ratio of the radius of the bounding surface to that of the cone is not too large ($< \frac{1}{3}$), the interpretation of experimental results on the basis of the infinite cone-and-plate system will be accurate to within 10%, but this error will grow rapidly as the intermediate inertial region disappears.

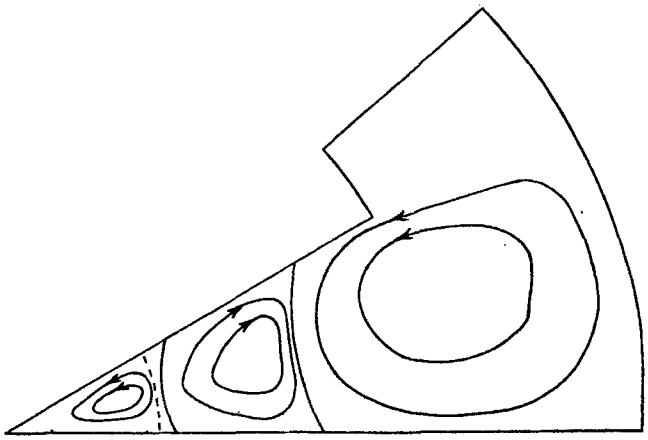

FIGURE 14. Streamline projections when $\theta_0 = 30°$, $\theta_d = 42°$, $\alpha_2' = -0{\cdot}03125$, $\alpha_3' = 0{\cdot}0625$ ($\Delta r = \frac{1}{80}$, $\Delta\beta = \pi/20$). – – –, The bounding region calculated on the basis of an infinite cone.

(iv) *Flow situations for small gap angles*

We now restrict ourselves to situations for which the angle between the cone and the plate is small. This is of particular interest, since one of the popular methods for characterizing the behaviour of elastico-viscous liquids utilizes the cone-and-plate geometry with a gap angle sometimes as high as 10° (J. Meissner, private communication), but usually less than 4°. At least one commercial rheometer, the Weissenberg Rheogoniometer (manufactured by Sangamo Controls Ltd.), is built on this principle.

The interpretation of results from the rheogoniometer is based on the following assumptions:

(i) The cone and plate are infinite in extent. This essentially implies that the state of steady shear flow existing in the gap is unaffected by the edge (cf. Adams & Lodge 1964; Coleman, Markovitz & Noll 1966).

(ii) The gap angle is very small and the rate of shear is constant in the gap.

(iii) Inertial forces and secondary flows may be neglected (i.e. $\chi_1 = 0$).

With these assumptions, the physical components of the stress tensor for the second-order fluid can be written in the form,

$$\left.\begin{aligned} p_{(rr)} &= -p, \\ p_{(\theta\theta)} &= -p+\gamma^2(2\alpha_2+\alpha_3), \\ p_{(\phi\phi)} &= -p+\gamma^2\alpha_3, \\ p_{(\theta\phi)} &= \gamma\alpha_1, \\ p_{(r\theta)} &= p_{(r\phi)} = 0, \end{aligned}\right\} \tag{40}$$

where the rate of shear γ is given by†

$$\gamma = -\Omega\sin\theta\frac{\partial w_0}{\partial\theta} = -2\Omega A_1\operatorname{cosec}^2\theta. \tag{41}$$

It can also be shown that the normal pressure on the stationary plate, $[-p_{(\theta\theta)}]_{\theta=\pi/2}$, is given by (cf. equation 39)

$$[-p_{(\theta\theta)}]_{\theta=\pi/2} = p_a - 2\gamma^2(\alpha_2+\alpha_3)\ln(r/a). \tag{42}$$

Differentiating (42) with respect to $\ln r$, we have

$$\frac{\partial}{\partial\ln r}[-p_{(\theta\theta)}]_{\theta=\pi/2} = -2\gamma^2(\alpha_2+\alpha_3). \tag{43}$$

From (43) we see that measurements of the slope of the $(-p_{(\theta\theta)}|_{\theta=\pi/2}, \ln r)$ curve can be used to determine $\alpha_2+\alpha_3$. Our theory is based on a flow which is sufficiently slow. In the general case (43) can be replaced by (cf. Adams & Lodge 1964; Walters 1968)

$$\frac{\partial[-p_{(\theta\theta)}]_{\theta=\pi/2}}{\partial\ln r} = -[\sigma_1+\sigma_2], \tag{44}$$

where the first and second normal-stress differences σ_1 and σ_2 are given by

$$\left.\begin{aligned} p_{(\phi\phi)}-p_{(rr)} &= \sigma_1(\gamma), \\ p_{(\theta\theta)}-p_{(rr)} &= \sigma_2(\gamma). \end{aligned}\right\} \tag{45}$$

The total normal force F on the plate $(0 \leqslant r \leqslant a)$ is given by

$$F = -2\pi\int_0^a p_{(\theta\theta)}|_{\theta=\pi/2}\, r\, dr, \tag{46}$$

which integrates to give

$$F = \pi a^2\gamma^2\alpha_2. \tag{47}$$

In the general case, this must be replaced by (Walters 1968)

$$F = \frac{\pi a^2}{2}[\sigma_1-\sigma_2]. \tag{48}$$

The total force F can therefore be used to determine $\sigma_1-\sigma_2$ (or α_2 within the restrictions of our theory).

† It has been shown (Walters and Waters 1968) that replacing γ by the constant value Ω/θ_0 introduces errors of the order of 0·25 % for a 4° gap.

Our main concern in § 4 (iv) is the influence of edge effects on couple, pressure and total-force measurements made under rheogoniometric conditions.† Under these conditions, the range of applicability of the theory is limited by the high shear rates usually encountered, which invalidate the second-order approximation. Here, the theory has predictive value only for very low rotational speeds. However, one would expect the conclusions concerning 'edge effects' to be a useful guide in a much wider context.

In the following, we shall not consider the effect of secondary flows or rheogoniometric measurements, since we have established, in agreement with the findings of Walters & Waters (1968) for the infinite cone-and-plate case, that these are in fact negligible.

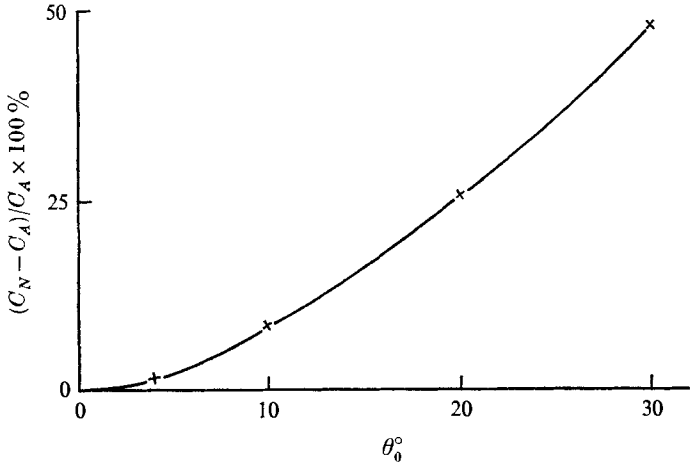

FIGURE 15. The percentage difference between C_N and C_A as a function of gap angle θ_0.

It has been shown earlier that, within the confines of the present theory, the limiting viscosity α_1 may be obtained from measurements of the couple C (cf. equation (25)). We shall take, as a measure of edge effects on this measurement, the difference between C_N and C_A, where C_N is the value of C given by (25) and (26), and C_A is the value of C given by (37) and (38).

In figure 15, we have plotted the percentage difference between C_N and C_A (i.e. $(C_N - C_A)/C_A \times 100$) as a function of gap angle. This graph may be useful to experimentalists in assessing the possible edge effects in couple measurements for a given gap angle. We see, for example, that the error is likely to be less than 2 % for cone angles of 4° or less.

For completeness, we extended the work of part 1 for the parallel-plate

† The most usual situation in cone-and-plate rheogoniometry is for the test fluid to occupy a finite volume and to be held in the gap by surface-tension forces. However, in some cases the cone is rotated in a sea of test fluid, as for example is the case when the Mooney plattens are used in conjunction with the Weissenberg Rheogoniometer (see also Adams & Lodge 1964; Kaye, Lodge & Vale 1968). Here, for mathematical convenience, we consider the second situation, in which case surface tension effects are not relevant.

geometry and computed the couple in an analogous way to that for the cone-and-plate geometry. Figure 16 contains the percentage error as a function of h/a, where h is the gap between the plates and a the radius of the rotating plate. The results are in good qualitative agreement with those given in figure 15 if we associate h/a with the gap angle θ_0.

We now focus attention on a more difficult facet of rheogoniometry, namely the determination of the normal-stress differences, which in our context implies the determination of α_2 and α_3. We neglect the effect of secondary flows and compare the values of $[-p_{(\theta\theta)}]_{\theta=\pi/2}$ obtained from (28) and (29) (with $\chi_1 = 0$) for the finite-cone situation with the values obtained from (39) (with $f = g = 0$) for the infinite-cone case, the arbitrary function of θ arising from integration of (28)

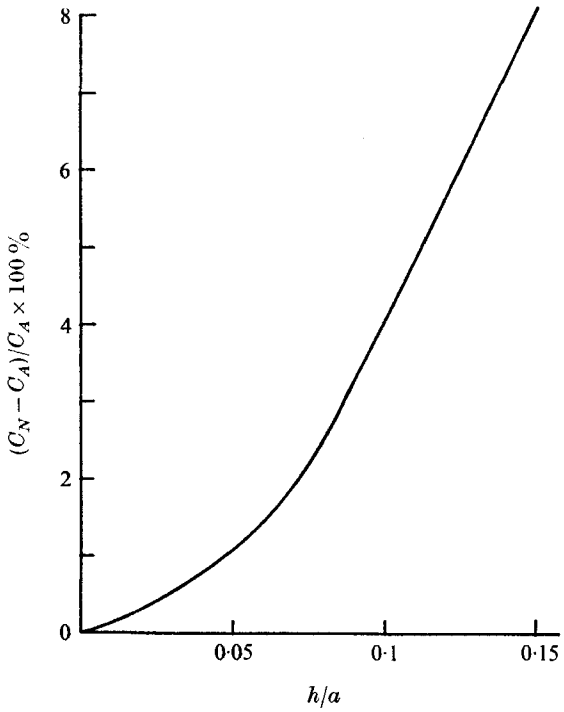

FIGURE 16. The percentage difference between C_N and C_A as a function of h/a.

being chosen to give the same pressures at $r = \Delta r$, $\theta = \pi/2$. This is permissible, since we are concerned here with the pressure *gradient* along the plate. Our choice has been governed by convenience of presentation of the results. Figures 17–19 contain this comparison for certain values of α_2' and α_3'. They show that, whereas the two curves diverge strongly for a 30° gap, the agreement, for 4 and 10° gaps, is good up to distances very close to the edge. This implies that the state of flow given by (33) and (35) is maintained almost up to the edge.

It is possible to assess edge effects in total normal-force measurements by comparing the values F_A of F obtained from (47) and the values F_N of F obtained by the numerical integration of (46) in the finite-cone case. However, we must

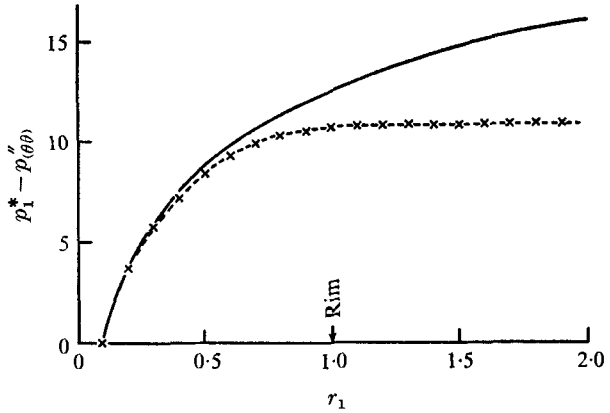

FIGURE 17. The radial variation of the non-dimensional normal pressure on the stationary plate for $\theta_0 = 30°$, $\alpha_2' = -1{\cdot}0$, $\alpha_3' = 2{\cdot}0$: – – –, based on numerical solution ($\Delta r = \frac{1}{15}$, $\Delta\theta = \pi/20$); ———, based on *infinite*-cone solution.

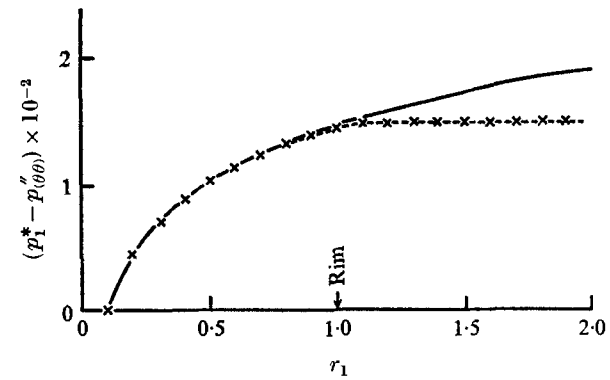

FIGURE 18. The radial variation of the non-dimensional normal pressure on the stationary plate for $\theta_0 = 10°$, $\alpha_2' = -1{\cdot}0$, $\alpha_3' = 2{\cdot}0$: – – –, based on numerical solution ($\Delta r = \frac{1}{15}$, $\Delta\theta = \pi/20$); ———, based on *infinite*-cone solution.

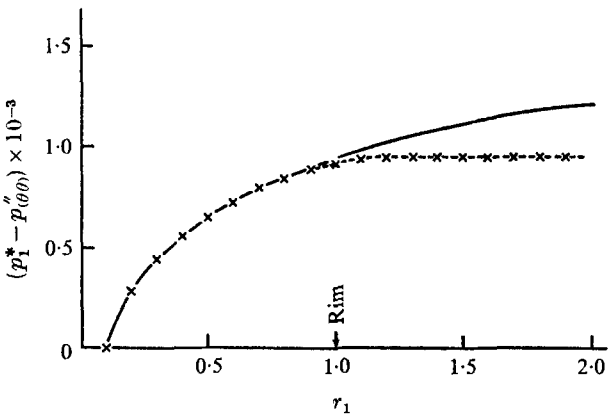

FIGURE 19. The radial variation of the non-dimensional normal pressure on the stationary plate for $\theta_0 = 4°$, $\alpha_2' = -1{\cdot}0$, $\alpha_3' = 2{\cdot}0$: – – –, based on numerical solution ($\Delta r = \frac{1}{15}$, $\Delta\theta = \pi/20$); ———, based on *infinite*-cone solution.

first consider the importance in this type of measurement of the arbitrary function of θ arising from the integration of (28). The precise form of this function will be determined by a number of factors including the type of shear-flow existing in the sea of liquid. We should not be surprised, therefore, if a change of flow conditions in the sea of liquid produces a corresponding change in the pressure $[-p_{(\theta\theta)}]$ on the plate. The increase or decrease in $[-p_{(\theta\theta)}]$ would be the same at all points of the plate, i.e. it would be independent of r.† We have already noted that this would not affect the pressure *gradient* on the plate, but it would affect the total force. When comparing F_A and F_N, we are therefore neglecting the influence of any shear flow in the sea of liquid, and are estimating the effect on total-force measurements of any departure from a state of steady-shear flow near the edge of the cone. Table 2 contains the non-dimensional total forces (F'_A and F'_N) for the infinite-cone and finite-cone situations for $\alpha'_2 = -1$

θ_0°	F'_A	F'_N
30	4·89	4·1
10	57·56	57·12
4	369·2	368·5

TABLE 2

and $\alpha'_3 = 2$ and various gap angles. We see that, whereas the percentage difference is about 10% for a 30° gap, it is very small for a 4° gap being of the order of a fraction of a percentage.

The numerical work of § 4 (iv) has indicated that in rheogoniometric situations with gap angles of less than 4°, the state of flow predicted on the infinite cone and plate assumption is valid over most of the flow field and edge effects appear to give rise to only small errors.‡

Hitherto, the pressure distribution method of determining normal-stress differences has been preferred to the total-normal-force method, since it has been argued that the individual pressure measurements can be taken at sufficient distances from the edge for edge effects to be negligible, whereas it is impossible to isolate edge effects in total-force measurements. In fact, these edge effects have sometimes been anticipated to be quite large (Markovitz 1965). The work of § 4 (iv) has indicated that this point of view is possibly over pessimistic, and that both pressure-distribution and total-force methods for determining normal-stress differences are not likely to be unduly affected by edge effects.

We are grateful to Mr R. Williams for assistance with the photography.

† This is in agreement with the experimental results of Kaye *et al.* (1968), who investigated the effect of varying the gap angle on $[-p_{(\theta\theta)}]_{\theta=\pi/2}$ for a given shear rate.

‡ Sample results obtained from an extension of the work of part 1 indicate that this conclusion is also valid for the parallel-plate case.

REFERENCES

ADAMS, N. & LODGE, A. A. 1964 *Phil. Trans.* A **256**, 149.

BHATNAGAR, P. L. & RATHNA, S. L. 1962 *Quart. J. Mech. Appl. Math.* **16**, **329**.

COLEMAN, B. D., MARKOVITZ, H. & NOLL, W. 1966 *Viscometric Flows of Non-Newtonian Fluids.* Berlin: Springer.

GIESEKUS, H. 1967 *Rheologica Acta*, **6**, 339.

GRIFFITHS, D. F., JONES, D. T. & WALTERS, K. 1969 *J. Fluid Mech.* **36**, 161.

KAYE, A., LODGE, A. S. & VALE, D. G. 1968 *Rheologica Acta*, **7**, 368.

MARKOVITZ, H. 1965 *Proc. 4th Intern. Congr. on Rheology* **1**, 189. New York: Interscience.

MOHAN RAO, D. K. 1963 *Proc. Ind. Acad. Sci.* **56**, 198.

THOMAS, R. H. & WALTERS, K. 1964 *Quart. J. Mech. Appl. Math.* **17**, 39.

WALTERS, K. 1968 *Basic Concepts and Formulae for the Rheogoniometer.* Sangamo Controls.

WALTERS, K. & WATERS, N. D. 1963 *Brit. J. Appl. Phys.* **14**, 667.

WALTERS, K. & WATERS, N. D. 1968 *Polymer Systems: Deformation and Flow.* London: Macmillan.

WATERS, N. D. 1964 *Brit. J. Appl. Phys.* **15**, 600.

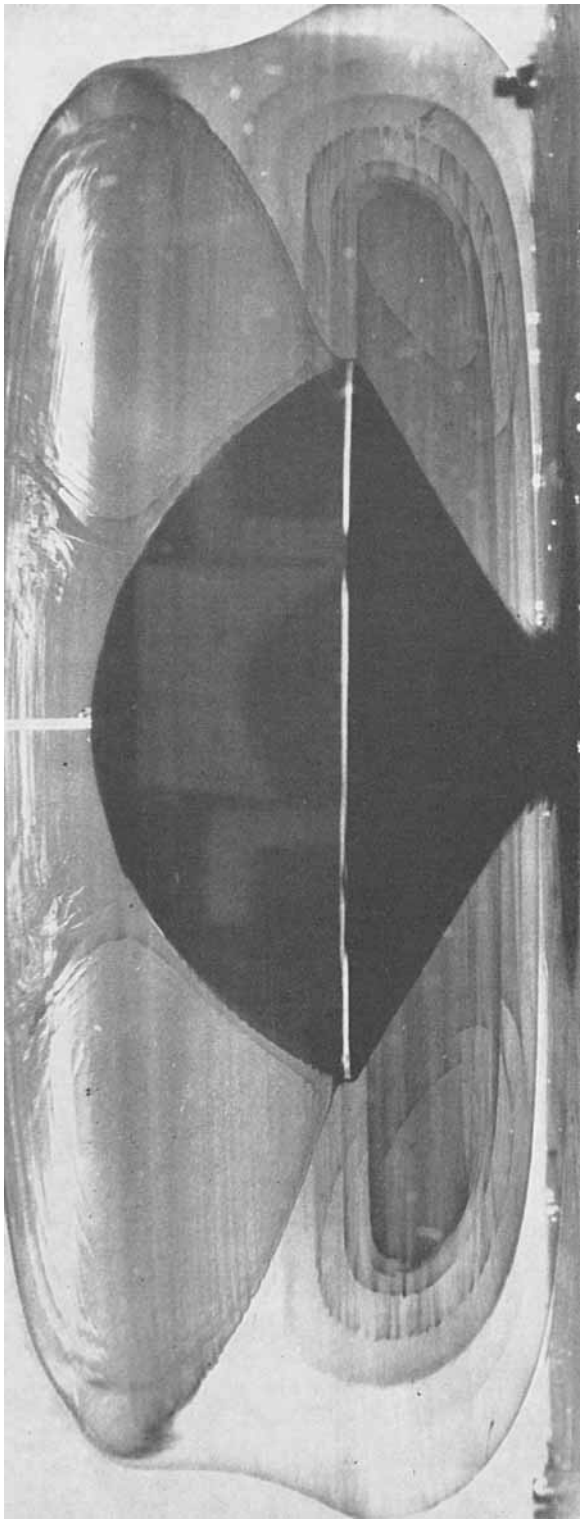

FIGURE 10. Streamlines for a Newtonian liquid (glycerol).

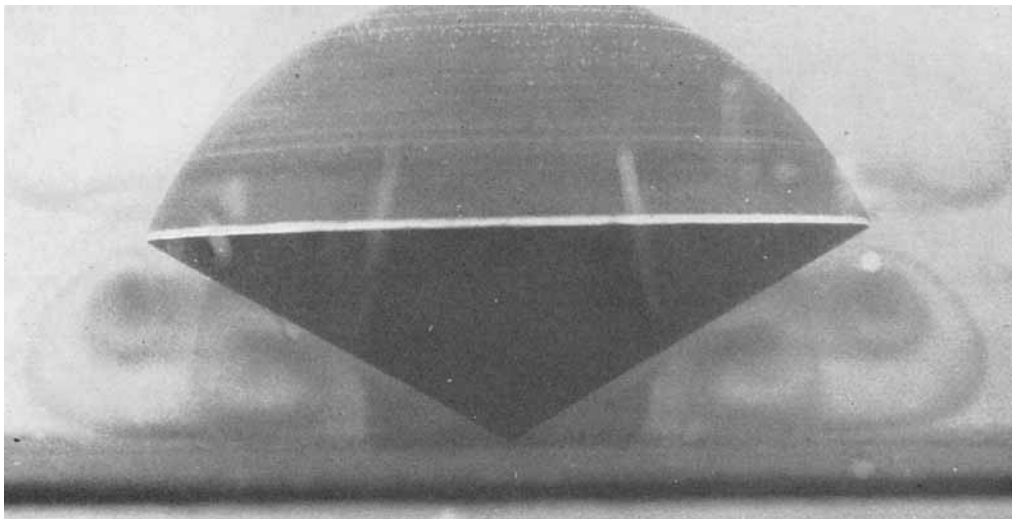

FIGURE 11. Streamlines observed when the cone (*with* spherical cap) is rotated in a 1·5% aqueous solution of polyacrylamide.

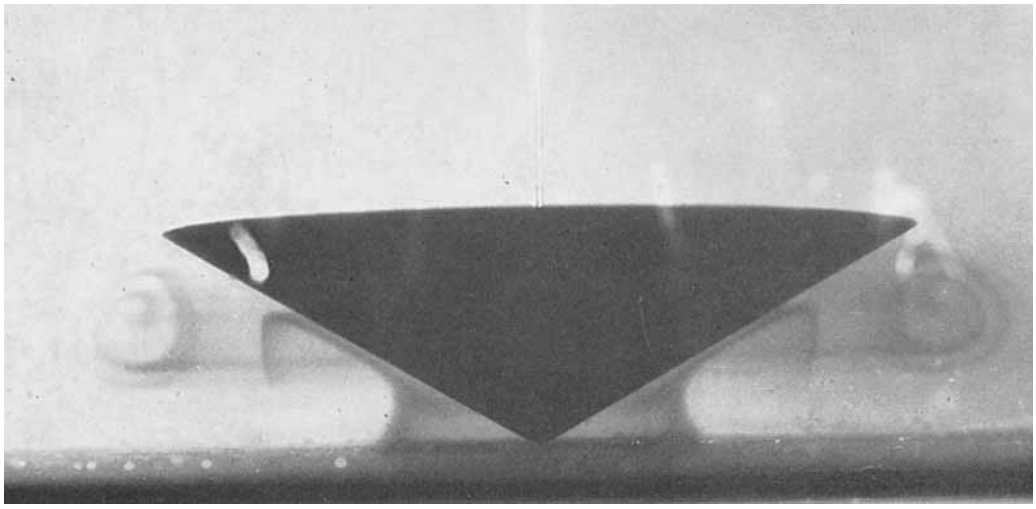

FIGURE 12. Streamlines observed when the cone (*without* spherical cap) is rotated in a 1·5% aqueous solution of polyacrylamide.

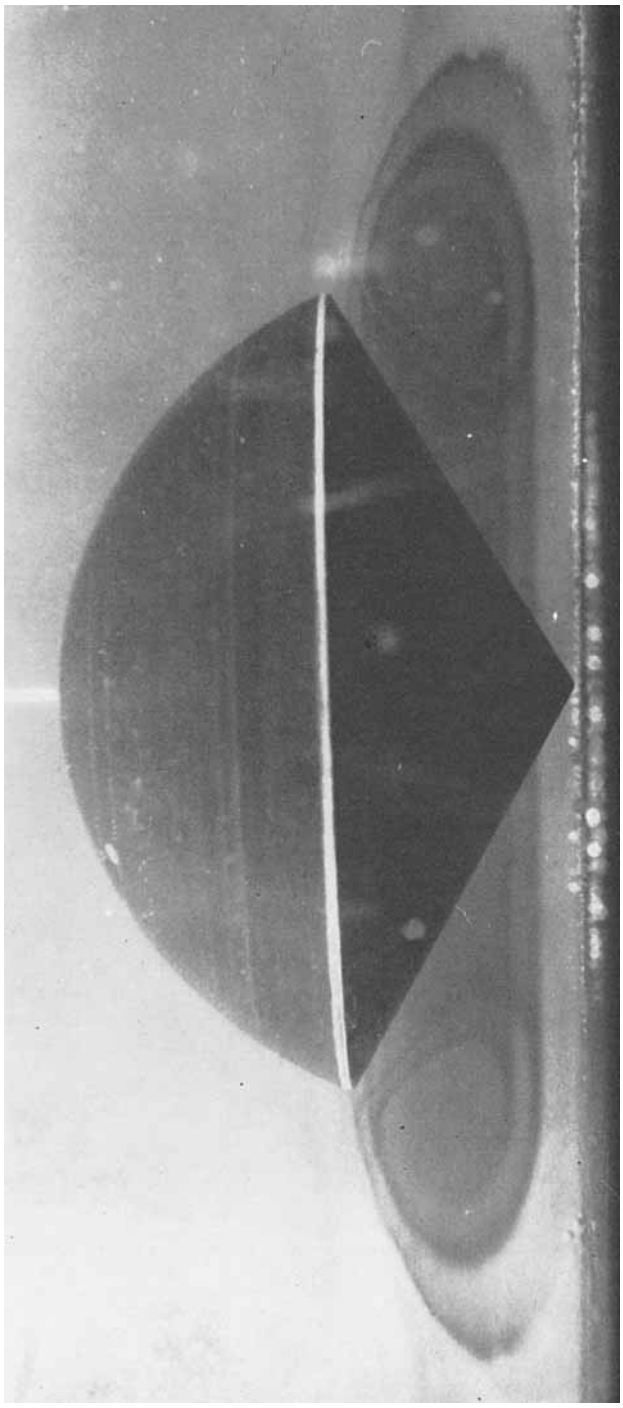

FIGURE 13. Streamlines observed for a 3·0% aqueous solution of polyacrylamide.